

SecBeam: Securing mmWave Beam Alignment against Beam-Stealing Attacks

Jingcheng Li, Loukas Lazos, Ming Li
University of Arizona
{jli2972, llazos, lim}@arizona.edu

Abstract—Millimeter wave (mmWave) communications employ narrow-beam directional communications to compensate for the high path loss at mmWave frequencies. Compared to their omnidirectional counterparts, an additional step of aligning the transmitter’s and receiver’s antennas is required. In current standards such as 802.11ad, this beam alignment process is implemented via an exhaustive search through the horizontal plane known as beam sweeping. However, the beam sweeping process is unauthenticated. As a result, an adversary, Mallory, can launch an active beam-stealing attack by injecting forged beacons of high power, forcing the legitimate devices to beamform towards her direction. Mallory is now in control of the communication link between the two devices, thus breaking the false sense of security given by the directionality of mmWave transmissions.

Prior works have added integrity protection to beam alignment messages to prevent forgeries. In this paper, we demonstrate a new beam-stealing attack that does not require message forging. We show that Mallory can amplify and relay a beam sweeping frame from her direction without altering its contents. Intuitively, cryptographic primitives cannot verify physical properties such as the SNR used in beam selection. We propose a new beam sweeping protocol called SecBeam that utilizes power/sector randomization and coarse angle-of-arrival information to detect amplify-and-relay attacks. We demonstrate the security and performance of SecBeam using an experimental mmWave platform and via ray-tracing simulations.

I. INTRODUCTION

Millimeter Wave (mmWave) communications are a key enabling technology for the Next-Generation of wireless networks [26], [39]. The abundance of available bandwidth offers unprecedented opportunities for high data rates, ultra-low latency, and massive connectivity. However, the short wavelength poses new challenges at the physical layer due to the substantial signal attenuation (which is proportional to the center frequency) and susceptibility to blockage [26]. To compensate for this high attenuation, mmWave devices employ high-gain directional transmissions which are possible due to the small antenna factor necessary at small wavelengths. New highly-directional antenna systems pack many antenna elements into a small area which can be electronically steered to form high-gain pencil like beams at any desired direction.

Compared to their omnidirectional counterparts, narrow-beam directional systems require continuous beam management [37]. The beam management process consists of the initial phase of beam alignment between the Tx and the Rx and the subsequent phase of beam tracking if any of the Tx or Rx are mobile, or the physical environment changes. Recent standards such as the IEEE 802.11ad [14] and its enhanced

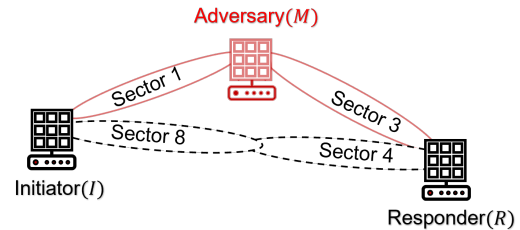


Fig. 1: Beam-stealing attack against the SLS protocol. I and R beamform towards the adversary instead of the LoS path.

version IEEE 802.11ay [11], describe beam alignment as an exhaustive search process called *sector-level sweep* (SLS) where all possible directions are scanned before the optimal Tx and Rx antenna orientations are decided. Specifically, one device acts as the *initiator* I , whereas the other acts as the *responder* R . The initiator sequentially sends sector sweep frames (beacons) in every candidate direction using narrow-beam transmissions while the responder receives in quasi-omni mode. The responder measures the received power from each receivable beacon and determines the initiator’s direction (sector) with the highest signal-to-noise ratio (SNR). The process is repeated in the opposite direction to define the responder’s sector with the highest SNR. Upon completion, the initiator’s and the responder’s beams are aligned to the direction that maximizes the cumulative antenna gain which can be a line-of-sight (LoS) path or a reflection path.

The beacons in the SLS protocol, however, are unauthenticated and can be easily forged. An adversary, Mallory, can launch an active beam-stealing attack by injecting forged beacons of high power, forcing the legitimate Tx and Rx to beamform towards her direction [30]. This attack is shown in Figure 1 where the initiator selects sector 1 instead of sector 8 and the responder selects sector 3 instead of 4. Mallory is now in control of the communication link between I and R , thus breaking the false sense of security given by the directionality of mmWave transmissions [18], [42]. She can eavesdrop on the link, apply traffic analysis to infer information from encrypted communications [22], inject and modify messages, or selectively drop them.

A few methods have been proposed to prevent beam-stealing attacks [4], [28], [31], [35], [36], [41]. Steinmetzer *et al.* introduced an authenticated beam sweep protocol [28]. The main idea is to prevent the forging of beacons by guaranteeing their authenticity and freshness via cryptographic means (e.g.,

encrypt and sign beacon transmissions). However, *we postulate that a beam-stealing attack is still feasible against an authenticated beam sweep protocol*. Specifically, we demonstrate a new amplify-and-relay attack that does not require access to cryptographic primitives on behalf of Mallory.

Amplify-and-relay beam-stealing attacks. To achieve beam-stealing when beacons are authenticated, Mallory can launch a relay attack as shown in Figure 1. When I transmits a beacon toward Mallory (sector 8), Mallory swiftly amplifies and relays the beacon toward the responder. Mallory does not need to decode the beacon or modify its contents, as the beacon only needs to be received at higher power. Because the beacon is generated by I and contains the correct authenticator, it passes authentication at R . Due to the signal amplification, R is led to believe that sector 8 yields the highest SNR and provides this feedback to I . The relay attack is repeated in the R to I direction, leading I to believe that the third sector of R yields the highest SNR.

The amplify-and-relay attack is feasible because the added cryptographic protections validate the contents of the beacons, but fail to authenticate the physical property used for sector selection which is the SNR. Practically, the attack distorts the wireless environment and cannot be dealt with by cryptographic means alone.

Existing relay attacks that aim at breaking proximity constraints (e.g., [8], [9]) are different from amplify-and-relay beam-stealing attacks in terms of goals and assumptions. Other known attacks of similar nature are signal cancellation attacks where a carefully placed adversary relays a transmitted signal with the purpose of causing destructive interference at the intended receiver [21], [23], which are harder to realize. An intuitive defense against relay attacks is to differentiate between the legitimate transmitter and the relay. Fingerprinting techniques such as those in [4], [35], [36] extract unique fingerprints from the devices such as antenna patterns, frequency offset and DC offset characteristics, etc. However, these methods require training, may utilize multiple access points and are not applicable when devices meet for the first time. Others, such as the angle-of-arrival-based detection method [41] and SNR fingerprinting methods [36] assume that the locations of the devices are fixed and known.

In this paper, we address the problem of securing the SLS protocol of 802.11ad against amplify-and-relay beam-stealing attacks. **Our main contributions are as follows:**

- We demonstrate a new amplify-and-relay attack against the beam alignment process of mmWave communications. This attack defeats cryptographic defenses that rely on beacon authentication to detect beacon forging.
- We develop an attack detection method that exploits the power-delay profile (PDP) of the mmWave channel. Assuming that the LoS path is available, any amplified relay path will have a longer delay and a higher SNR compared to the LoS path. However, a signal traveling through the LoS path should incur the least attenuation due to its free space propagation over a shorter distance.

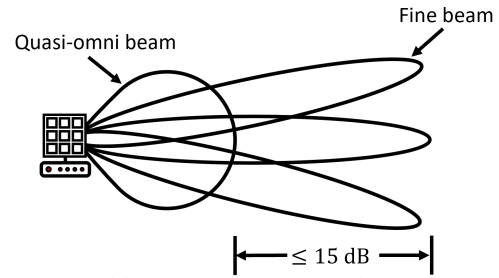


Fig. 2: A steerable mmWave antenna that can operate in fine-beam mode or quasi-omni mode.

We use the discrepancies in the PDP to detect amplify-and-relay attacks over paths longer than the LoS path.

- The PDP detection method assumes the presence of the LoS path, which may not be true. To generalize attack detection to all environments, we propose the SecBeam protocol that derives security from a combination of power randomization and coarse AoA detection. The focal idea is to hide the sector identity and randomize the beacon transmit power to prevent Mallory from fine-tuning her amplification power. Without knowledge of the sector ID and transmit power, Mallory has to amplify the beacons from all sectors she can hear. This leads to a disproportionate number of beacons arriving from the same direction, violating the geometrical mmWave channel model [15]. SecBeam requires minimal modifications to the original SLS protocol of 802.11ad.
- We analyze the security of SecBeam and show that it can detect an amplify-and-forward attacker that relays incoming beacons at fixed transmit power or at fixed amplification. We experimentally evaluate the performance and security of SecBeam on a 28GHz mmWave testbed in typical indoor environments. Our experiments demonstrate that SecBeam allows legitimate devices to optimally align their beams while detecting amplify-and-relay attacks with high probability.

II. THE SLS PROTOCOL IN IEEE 802.11AD AND ATTACK

A. The SLS protocol in IEEE 802.11ad

The beam alignment process in the IEEE 802.11ad, also known as “sector-level sweep (SLS)”, aims at maximizing the combined Tx-Rx antenna gain [14]. This is done by sweeping the plane using fine-beam and quasi-beam antenna configurations and identifying the directions (sectors) of optimal antenna alignment. Sweeping is achieved electronically by controlling the individual antenna elements [10]. An example of a steerable antenna pattern is shown in Figure 2. The antenna can be set to quasi-omni mode for wider coverage, or to a fine-beam mode for the highest gain.

The main idea of SLS is shown in Figure 3. One device assumes the role of the initiator (I) whereas the other assumes the role of the responder (R). The initiator sets its antenna in fine-beam mode and sweeps through the plane transmitting sector sweep frames (SSF). The receiver operates in quasi-omni mode, recording the received SNR from each sector as

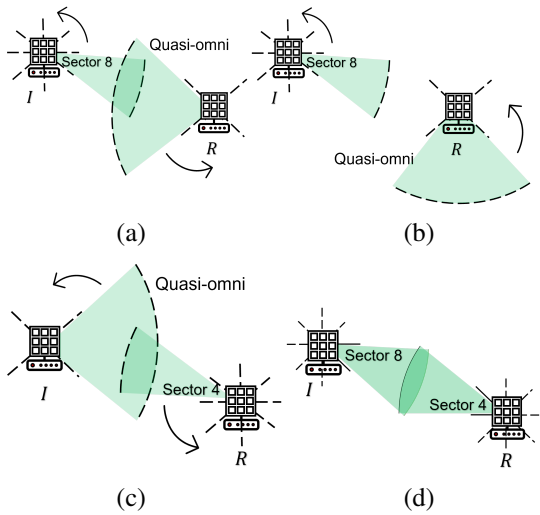


Fig. 3: The SLS process of 802.11ad: (a) I sweeps through the plane in fine-beam mode while R receives in quasi-omni mode, (b) I repeats the sector sweep for every quasi-omni pattern of R , (c) R sweeps through the plane in fine-beam mode while I receives in quasi-omni mode, (d) The antennas of I and R are optimally aligned.

shown in Figure 3(a). In the next phase, the two devices switch roles. The responder transmits in fine-beam mode while the initiator is in quasi-omni mode. Additionally, the responder provides feedback about the optimal initiator's sector (highest SNR), as recorded from the previous phase. Finally, the initiator provides feedback to the responder about the optimal responder's sector and the two antennas are aligned as shown in Figure 3(b). In detail, the SLS protocol consists of the three phases shown in Figure 4(a).

Initiator sector sweep phase.

- 1) The plane is divided into N sectors S_1, S_2, \dots, S_N . The initiator I sweeps through each S_i and transmits sector sweep frame (SSF) $SSF_I(i)$, using the fine-beam mode.
- 2) The responder R measures the SNR for each received SSF, while in quasi-omni mode.
- 3) Steps 1 and 2 are repeated for every quasi-omni antenna orientation in R to cover R 's plane. The responder records the sector S'_I with the highest SNR.

Responder sector sweep phase.

- 4) The responder switches to fine-beam mode whereas the initiator switches to quasi-omni mode. The responder R sweeps through each sector S_i and transmits $SSF_R(i)$, using the fine-beam mode. Further, the responder populates the sector sweep (SSW) feedback field of the SSF with the I 's optimal transmitting sector S'_I , as identified in the previous phase.
- 5) The initiator records the sector S'_R with the highest received SNR and also learns S'_I from R 's feedback.

Acknowledgement phase.

- 6) The initiator sends a SSW-Feedback frame to R indicating R 's optimal transmitting sector S'_R . The feedback is

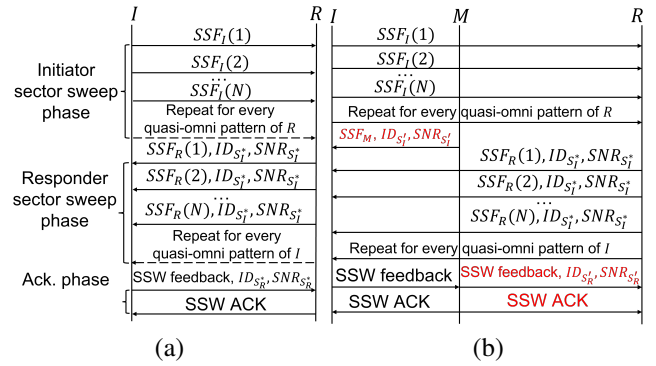


Fig. 4: (a) SLS protocol in IEEE 802.11ad standard, (b) beam-stealing attack against SLS protocol

transmitted in fine-beam mode using sector S'_I , whereas the responder is in quasi-mode.

- 7) At the last step, the responder transmits a sector sweep ACK to the initiator using sector S'_R .
- 8) The two antennas are aligned at the S'_I - S'_R direction.

In the example of Fig. 3, the responder identifies $S'_I = S_8$ whereas the initiator identifies $S'_R = S_4$. The two devices use the $S_8 - S_4$ antenna orientation for communications.

B. Beam-Stealing Attack Against the SLS Protocol

In this section, we describe the beam-stealing attack against SLS protocol in IEEE 802.11ad presented by Steinmetzer et al. [30]. The attack is launched by M who forges the SSF frames. The timeline of the attack is shown in Fig. 4(b).

Mallory positions herself within range of both I and R (though the attack can be also launched by two colluding devices). During the initiator sector sweep phase, Mallory measures the SNR from all sectors of I and chooses the one that yields the highest SNR, denoted by S'_I . Because the communication protocol lacks an authentication mechanism, Mallory impersonates R by forging R 's SSFs and indicating S'_I as the best sector. The same process is repeated during the responder sector sweep phase, where M chooses the best sector S'_R and informs R through forged SSF frames on behalf of I . Ultimately, I and R choose sectors S'_I and S'_R that beamform towards M , as illustrated in Figure 1. I and R choose sectors S_1 and S_3 instead of S_8 and S_4 . Mallory gains full control over the communication between the victim devices, enabling a range of potential attacks such as eavesdropping, traffic analysis, data modification and injection.

C. Authenticated Beam Sweeping

It is evident that the beam stealing attack is possible due to the lack of authentication and integrity protection on the SSF frames. To counter this vulnerability, Steinmetzer et al. proposed an authenticated version of SLS where I and R are assumed to possess public/private key pairs [28] which are used to securely establish a session key s . The session key is used for mutual authentication and freshness to protect against message forgeries and replay attacks. Specifically, during the initiator sector sweep phase, I generates a unique

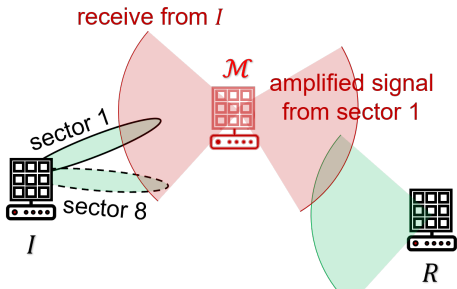


Fig. 5: Amplify-and-relay attack. \mathcal{M} receives an authentic SSF while I is scanning sector 1. \mathcal{M} amplifies and relays the SSF without decoding. The responder authenticates the SSF and perceives sector 1 to yield the highest SNR.

cryptographic nonce v_I that is sent with every SSF frame. R receives the SSF frames, determines the best sector S_I^* , and computes an authenticator α_R of length l_α as

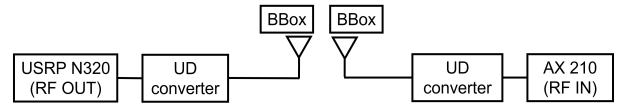
$$\alpha_R = \text{auth}_{l_\alpha}(S_I^*, v_I, s) = \text{trunc}(h(S_I^*, v_I, s), l_\alpha),$$

where $\text{auth}_{l_\alpha}(S_I^*, v_I, s)$ computes an authenticator of size l_α as a truncated hash function of the concatenation of S_I^* , v_I and s . In the responder sweep phase, R generates a nonce v_R . The initiator computes its authenticator as $\alpha_I = \text{auth}_{l_\alpha}(S_R^*, v_R, s)$ for the optimally selected sector S_R^* . After both devices complete their sweeps, I sends S_R^* and α_I in a feedback frame and R acknowledges with S_I^* and α_R . Finally, both devices verify the received authenticators. If both verifications are successful, I and R set their sectors accordingly. Without access to the shared secret s , \mathcal{M} cannot create a forgery. Moreover, the nonces v_I and v_R guarantee freshness.

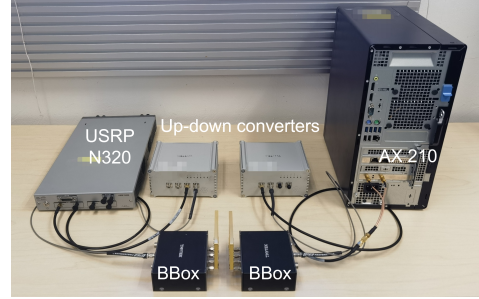
III. AMPLIFY-AND-RELAY BEAM-STEALING ATTACK

The authenticated beam sweep protocol proposed in [28] is still vulnerable to beam stealing attacks. This is because the cryptographic protections cannot prevent Mallory from *forging the wireless environment* by simply amplifying authentic SSFs. We present a new type of attack that we call *amplify-and-relay beam stealing* that allows Mallory to attract I 's and R 's beams without access to the shared secret s .

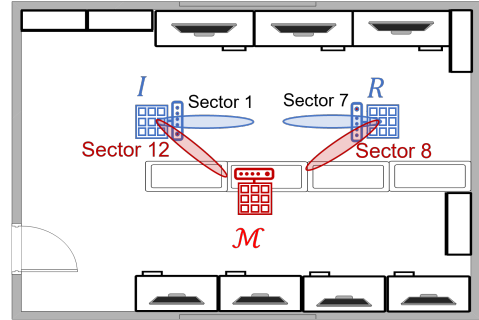
The attack operates as follows. Mallory positions herself at some location between I and R away from the LoS (we later examine Mallory's candidate attack locations). Mallory is equipped with two directional antennas (or a patch antenna that can operate two beams), which point towards the general direction of I and R , respectively. These antennas operate in quasi-omni mode to allow reception of I and R 's transmissions, as Mallory may not know the exact position of the two devices and the wireless environment (e.g., blockage). During the initiator sweeping phase, Mallory receives an authenticated SSF using the antenna pointing to I , amplifies it, and relays it intact with the antenna pointing to R . The responder authenticates the SSF and records the highest SNR from \mathcal{M} 's direction due to the applied amplification. The same amplification and relay is applied in the opposite direction during the responder sweep frame phase, leading I to indicate \mathcal{M} 's direction as the best one for beam alignment.



(a) RF chain of I and R



(b) Hardware used in the platform



(c) Experimental topology

Fig. 6: The mmWave experimental platform.

We emphasize that although timely relay of the SSFs is helpful, it is not necessary. First, the SLS protocol does not specify stringent timing constraints between the transmission of successive SSFs at different sectors. Second, some SSFs are not ever received by the intended receiver (I or R) due to antenna misalignment. Therefore, even if the relayed message arrives late, it is not a replay of the direct transmission and freshness is not violated.

Mallory can follow two amplification strategies when launching the beam stealing attack. The first is the *fixed power (FP)* strategy in which \mathcal{M} relays received signal(s) at a fixed transmit power, regardless of the received power. The closer distance of \mathcal{M} to I and R (if \mathcal{M} is in between) or a higher transmit power than the legitimate devices guarantees that \mathcal{M} 's relayed SSFs will be received with the highest SNR. However, if Mallory transmits at fixed power for all incoming SSFs, the receiver will measure the same SNR for several transmit sectors leading to easy attack detection. To succeed in her attack, Mallory may relay at high power only one SSF that she received. An alternate strategy is to apply *fixed amplification (FA)* to any incoming SSF leading at varying received power at the receiver. The main benefit of the *FA* strategy is that the received SNR is maximized when the transmitter (I or R) is best aligned with \mathcal{M} (due to the highest received power at \mathcal{M}) leading to a natural alignment of I and R with \mathcal{M} .

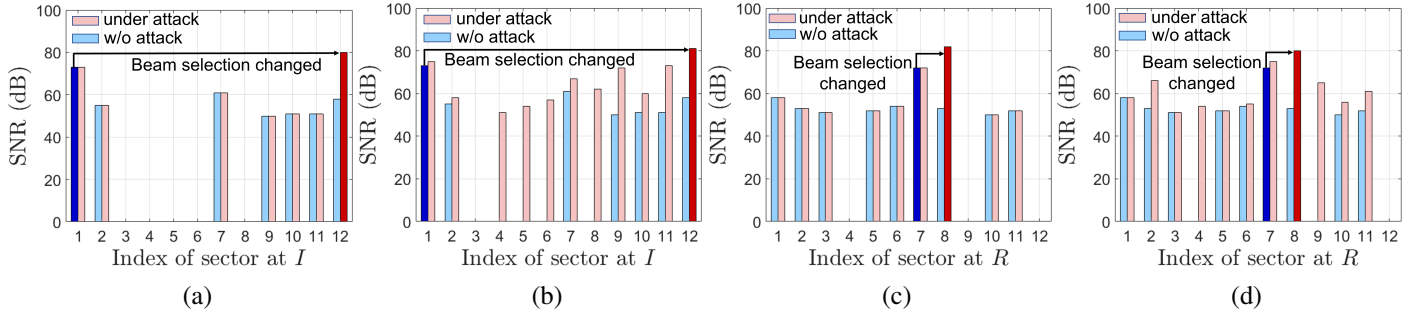


Fig. 7: (a) Amplify-and-relay beam-stealing attack on the initiator sector sweep using FP strategy, (b) attack on the initiator sector sweep using FA strategy, (c) attack on the responder sector sweep using FP strategy, (d) attack on the responder sector sweep using FA strategy.

A. Demonstration of the Amplify-and-Relay Attack

In this section, we experimentally demonstrate the amplify-and-relay attack.

Experimental Setup. Our experimental setup consisted of USRPs and Wi-Fi cards connected to the TMYTEK mmWave platform. Specifically, we implemented the baseband functionality of the initiator and Mallory on two Ettus USRP N320s [1]. Each USRP was connected to a TMYTEK up-down (UD) converter [2] that upsampled the signal from the sub-6GHz to a center frequency of 28GHz with 160MHz bandwidth. Transmission took place via a directional BBox lite patch antenna with 16 elements. The antenna supports electronically steerable sectors with half-power beamwidth of 30° , covering the plane with 12 non-overlapping sectors. The maximum transmit power of the USRPs was 30dBm. The platform configuration is shown in Fig. 6.

The responder was implemented with an AX 210 Wi-Fi card to allow for the extraction of CSI measurements by the PicoScience CSI tool [16]. The signal was received using the BBox lite antenna and downconverted to the sub-6 GHz band using the UD converter. The card extract CSI measurements and computed the RSS. Moreover, we used the Wi-Fi card to measure the noise floor, which remained consistent at -128 dBm throughout all the experiments. All hardware was controlled by a desktop computer and synchronized using the Ettus OctoClock-G module.

The experimental topology is shown in Fig. 7(a). We positioned all three devices in a laboratory of rectangular shape with typical office furniture (bookcases, desks with workstations, whiteboards, etc.) I and R were placed 4.3m apart whereas \mathcal{M} was placed in between (but not in the LoS) at distances 2.4m and 2.7m from I and R , respectively. To mimic the SLS protocol in IEEE 802.11ad as we described in Section II-A, we fixed the R 's beam and employed the TMXLAB Kit to electronically steer I 's beam. The transmitter conducted a 360° sweep of the entire plane. Upon completion of one sweep, R switched to the next fixed receive direction while I repeated the sweep. This sector sweep process was repeated in the other direction (with I and R switching roles) to determine the optimal beam of R .

During a fixed power attack, the legitimate devices and

Mallory transmitted at 10dBm, whereas during a fixed amplification attack, \mathcal{M} amplified its received signal by 70dB. Mallory was synchronized with the initiator and the responder via the the Ettus OctoClock-G module and transmitted the same SSF frame at the same time as the initiator or the responder (depending on the round).

Attack Evaluation. In Fig. 7, we show the highest measured SNR at the responder during the initiator sweep phase. Figure 7(a) corresponds to a fixed power attack. Without an attack, the responder measures the highest SNR when the initiator transmits at sector 1. During the attack, Mallory only amplified beam sector 12 that is best aligned towards her. Therefore, the responder measures the same SNR in all other sectors except sector 12, where the SNR is about 10dB higher than that of sector 1. This results in informing I that its best transmitting sector is sector 12, thus beamforming towards \mathcal{M} . Figure 7(b) shows the fixed amplification attack case that causes the same optimal sector change as the FP attack. One main difference is that during an FA attack, all sectors are amplified at the same gain thus causing an elevated SNR at R compared to the absence of the attack.

Figures 7(c) and 7(d) show the FP and FA attacks launched during the responder sector sweep phase. In both attacks, the beam selection shifts from sector 7 to sector 8 pointing to \mathcal{M} instead of the LoS. *We note that when I and R use sectors 12 and 8 respectively, they can no longer directly communicate.* The only way to communicate is via \mathcal{M} . To verify the generality of the attack with respect to the adversary positioning, we repeated the experiments with \mathcal{M} placed behind the initiator. The results of the second setup verify the attack feasibility and are presented in Appendix A.

IV. A BASELINE DEFENSE METHOD

We first propose a baseline method for detecting amplify-and-relay attacks that exploits the invariable physical properties of propagation time. The main idea is to use the longer signal propagation and processing times of the relay path over the legitimate path. This method is specifically applicable to the mmWave environment where multipath is limited. We use power delay profile (PDP) analysis to measure the timing of various paths and correlate it to the received power. As the mmWave signal attenuates rapidly with distance, it is expected

that the LoS path is the strongest and takes the least delay to propagate to the receiver. Detecting high SNR at a path with higher delay is indicative of an amplify-and-relay attack, provided that the LoS path (or any other shorter path) is unobstructed.

The PDP can be derived from the receiver’s channel impulse response (CIR) [25]. Let $X(f, t)$ and $Y(f, t)$ be the transmitted and received signals in the frequency domain and $H(f, t)$ be the CSI. Then $H(f, t)$ can be expressed as

$$H(f, t) = \frac{Y(f, t)}{X(f, t)} = e^{-j2\pi\Delta f t} \sum_{k=1}^N a_k(f, t) e^{-j2\pi f \tau_k(t)},$$

where $e^{-j2\pi\Delta f t}$ is the phase shift caused by the carrier frequency difference Δf between I and R , N is the number of paths, $e^{-j2\pi f \tau_k(t)}$ is the phase shift caused by the delay $\tau_k(t)$ of the k^{th} multipath, and $a_k(f, t)$ is the amplitude of the k^{th} multipath. Then the CIR, $h(t, \tau)$ can be calculated by applying an IFFT to the CSI,

$$h(t, \tau) = \sum_{k=1}^N a_k(t, \tau) e^{-j\theta_k(t, \tau)} \delta[\tau - \tau_k(t)],$$

where $e^{-j\theta_k(t, \tau)}$ is the phase shift and $\delta[\cdot]$ is a delta function. If choosing a time period equal or smaller than the channel’s coherence time, the CIR can be considered to be constant. Then the amplitude of the CIR, $|h(\tau)|$, can be extracted as,

$$|h(\tau)| = \sum_{k=1}^N a_k(\tau) \delta(\tau - \tau_k),$$

and the PDP is $|h(\tau)|^2$. Instead of using the PDP of each transmit sector directly, we apply an additional step to calculate the *collective power delay profile (CPDP)*. Specifically, we extract the amplitude and time delay of the *highest amplitude path* from the PDP of each SSF transmission and combine them in a single CPDP. This combination is possible only if time can be measured at high accuracy (which is possible at mmWave due to the available bandwidth) and if SSFs are transmitted periodically at precisely known times. In benign scenarios, the first peak of the CPDP corresponds to the LoS path between legitimate users. The signal strength received from this path is expected to be the strongest among all possible sectors. If a path that appears later has a stronger RSS, an attack is detected. Note that any reflections in mmWave not only travel longer distances, but also experience high attenuation due to the lower reflection coefficients as the small wavelength is comparable to surface imperfections.

Numerical Examples. We utilized the ray-tracing-based simulator mmTrace [29] to provide an illustration of how to employ CPDP to detect relay attacks in the initiator sector sweep. The topology under consideration is depicted in Fig. 8. The distances between devices are $d_{IR} = 5m$, $d_{MR} = 4.1m$ and $d_{IM} = 4m$. The initiator (I) is configured with $N = 32$ sectors with a HPBW of 12° , while the responder (R) is equipped with six non-overlapping quasi-omni patterns with

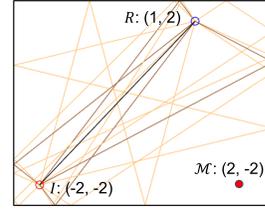


Fig. 8: Topology.

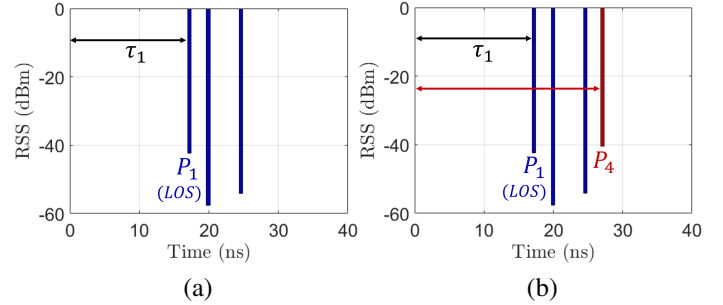


Fig. 9: CPDP: (a) without attack, the first peak is the strongest. (b) with a beam-stealing attack, the fourth peak is the strongest.

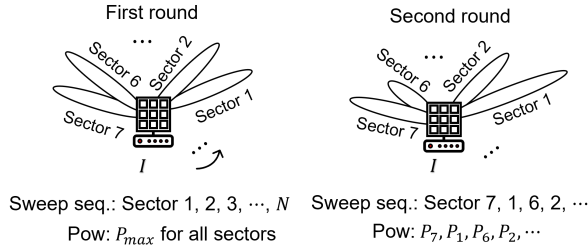
an HPBW of 60° . I conducts an SLS sweep for each quasi-omni pattern, while R measures the PDP for each transmit sector and extracts the highest amplitude path from each PDPs to create CPDP. If R observes multiple peaks with the same delay in different quasi-omni patterns, he chooses the one with the highest RSS.

The results of CPDP without attack is illustrated in Fig. 9(a). It is observed that the signals arriving later are weaker than the first peak as they travel along longer paths. However, in the presence of a beam-stealing attack (Fig. 9(b)), the fourth peak is stronger than earlier peaks, even though it comes from a longer path. This is due to the adversary amplifying and relaying the signal on that path. In such a scenario, R can detect the attack and reject the signal from I . Note that our results do not include any processing delays due to relaying.

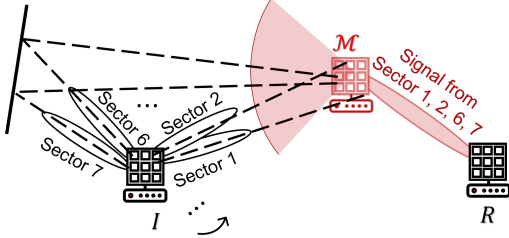
It should be noted that Mallory could avoid detection if it lies in the LoS path. However, the beam-stealing attack is not meaningful because the beams of I and R will lie in the optimal path and I and R can directly communicate unless \mathcal{M} introduces physical blockage. Moreover, this method does assume the existence of a faster path (e.g. LoS) than the adversary’s relay. Finally, the stringent synchronization requirement for computing the CPDP may require custom hardware [27]. To address these limitations, we propose an alternative protocol based on path loss and AoA.

V. THE SECBEAM PROTOCOL

We propose SecBeam, a secure beam sweeping protocol that detects amplify-and-relay attacks. To thwart fixed power amplification attacks, SecBeam implements a *physical-layer commitment scheme* where a transmitter commits to use the same power level over successive transmission rounds. Moreover, SecBeam incorporates coarse angle-of-arrival (AoA)



(a) Physical layer commitment



(b) Coarse AoA detection

Fig. 10: Overview of the SecBeam protocol: (a) the two sector sweep rounds of the SecBeam protocol and (b) when \mathcal{M} relays all sectors it hears, R receives multiple SSFs over the same receiving sector, indicating the same coarse AoA.

information to detect fixed amplification attacks. To motivate the SecBeam design, we first provide an overview of the focal ideas and follow with a detailed protocol description.

A. Overview

The main challenges in detecting an amplify-and-relay attack are that (a) cryptographic operators are not violated during a signal relay and (b) I and R do not have any prior knowledge of their relative positions and of the wireless environment. Without this information, a receiver cannot detect if a physical property such as SNR has been altered.

Physical layer commitments. To counter fixed power attacks, we construct a physical-layer security primitive that resembles a commitment scheme. We extend the SLS protocol to operate in two rounds. During the first round, I sweeps across each beam sector S_i sequentially using maximum power P_{\max} . The responder R calculates the path loss at round 1 as $PL_i(1) = P_i^T(1) - P_i^R(1)$ by subtracting the received power from the transmit power (in dB) using $P_i^T(1) = P_{\max}, \forall i$. This round serves as a *physical commitment* to the wireless environment even if this environment is distorted by Mallory.

During the second round, I repeats the sector sweep with two randomizations in place. First, I randomizes the sector sweeping sequence so it is no longer sequential. Second, I randomizes the transmit power on every sector. The sector ID S_i and the transmit power $P_i^T(2)$ are included in the SSF (which is encrypted). The responder calculates the path loss at round 2 and verify that $PL_i(1) \approx PL_i(2), \forall i$. This round serves as a *physical decommitment*, where the transmit power $P_i^T(2)$ and sector ID S_i are used to physically verify the

commitment of the first round. An example of the two-round sector sweep is shown in Fig. 10(a).

The power and sweeping sequence randomization have two effects on Mallory's attack. If Mallory amplifies both rounds at fixed power, the path loss computed by R would be different between the two rounds, thus revealing the attack. Mallory could attempt to detect the potentially lower received power from I . However, the randomization of the sweeping sequence and encryption of the sector ID does not allow Mallory to infer which sector it is receiving from at each round. Since Mallory does not know which sector in the second round corresponds to the one she relayed in the first round she could not fine tune its transmit power to make the path loss consistent across both rounds. The only strategy that is viable is **to amplify all sectors** overheard at \mathcal{M} with fixed amplification, that is, to launch a fixed amplification attack.

Coarse AoA detection. To counter fixed amplification attacks, we exploit another physical layer phenomenon that arises in the presence of a relay. Because Mallory is forced to apply a fixed amplification to all sectors (SSFs) it hears, an unusually high number of sectors will appear to arrive from the same direction. That is, although the initiator is sweeping the plane, the signal arrives to the responder from the same direction, thus indicating the presence of a relay. In the example of Fig. 10(b), sectors 1, 2, 6, and 7 all appear to be received at the same sector of R . To extract AoA information without requiring the application of complex AoA estimators such as MUSIC [13] during the sweeping process, R uses the quasi-omni mode to roughly estimate the incoming direction of a received signal. As the quasi modes are switched, R can calculate for how many transmitting sectors each quasi-omni receiving sector appears to be the optimal. It can then use those statistics for detecting relays.

B. Protocol details

We now present the detailed steps of the SecBeam protocol. The protocol is facilitated by a shared secret s established between I and R using public keys, as described in [28].

First round initiator sector sweep.

- 1) The initiator and the responder derive keys k_1 and k_2 from the shared common secret s . Key k_1 is used for integrity protection and k_2 is used for encryption.
- 2) The initiator sweeps through sectors S_1, S_2, \dots, S_N in this order and transmits sector sweep frame $SSF_i^I(1)$ at each S_i , using the fine-beam mode. Each $SSF_i^I(1)$ contains an authenticator $\alpha_i(1) = \text{MAC}(S_i, P_i^T(1), v_i(1), k_1)$, where MAC is a message authentication code function, $P_i^T(1)$ is the transmission power of $SSF_i^I(1)$ and $v_i(1)$ is a nonce. The initiator attaches $\alpha_i(1), P_i^T(1), v_i(1)$ to $SSF_i^I(1)$, encrypts it with k_2 and transmits it at power $P_i^T(1) = P_{\max}$.
- 3) The responder decrypts $SSF_i^I(1)$ using key k_2 and verifies the authenticator $\alpha_i(1)$ using k_1 . The responder records the path loss $PL_i(1) = P_{\max} - P_i^R(1)$, where $P_i^R(1)$ is the received power from sector S_i .

- 4) The responder finds the sector with the smallest path loss (highest SNR) as $S_I^*(1) = \arg \min_i PL_i(1)$.

First round responder sector sweep.

- 5) The initiator and the responder switch roles and repeat steps 1) to 4). Each sweep frame $SSF_i^R(1)$ includes the best sector S_I^* and the path loss vector $PL(1) = \{PL_1(1), PL_2(1) \dots PL_N(1)\}$ in the SSW feedback field.

Second round initiator sector sweep.

- 6) The initiator calculates the transmission power range for each sector S_i as $r_i : [P_{i,\min}, P_{\max} - \epsilon]$. Here, $P_{i,\min}$ is the minimum transmission power that allows decoding at R and is calculated as $P_{i,\min} = P_f + PL_i(1)$, where P_f is the receiver's sensitivity. Parameter ϵ is the expected path loss variation over the same path.
- 7) The initiator perturbs the sector sweep sequence $S = \{S_1, S_2, \dots, S_N\}$ using a pseudorandom permutation Π . The initiator sweeps through the N sectors using sequence $\Pi(S)$.
- 8) For each sector S_i , I randomly selects the transmission power $P_i^T(2) \in r_i$, calculates authenticator $\alpha_i(2)$, attaches $\alpha_i(2)$, $P_i^T(2)$, $v_i(2)$, and S_i to $SSF_i^I(2)$, encrypts it with k_2 and transmits it with power $P_i^T(2)$.
- 9) **Path loss test:** The responder decrypts the $SSF_i^I(2)$ using key k_2 and verifies the authenticator $\alpha_i(1)$ using k_1 . The responder records the path loss $PL_i(2) = P_i^T(2) - P_i^R(2)$, where $P_i^R(2)$ is the received power from sector S_i during the second round. If $|PL_i(1) - PL_i(2)| > \epsilon$, R detects an attack and aborts the protocol. Parameter ϵ is the same expected path loss variation over the same path as in Step 6.
- 10) **Coarse AoA test:** The responder records the quasi-omni receive sector that experiences the least path loss from each transmit sector S_i . It maintains the fraction of sectors heard at each receive sector as $F = \{f_1, f_2, \dots, f_L\}$, where L is the total number of quasi-omni sectors that cover the plane. If $f_j > \beta \cdot N$, $j = 1, 2, \dots, L$, R detects an attack and aborts the protocol.

Second round responder sector sweep.

- 11) The responder and the initiator switch roles and repeat steps (6) to (10).

C. Security Analysis of SecBeam

Forgery attacks. The original SLS protocol is susceptible to forgery attacks where Mallory can forge SSFs and change the feedback field on the optimal transmitting beam [30]. Such attacks are prevented in SecBeam due to the addition of integrity protection on the SSFs. Without access to the shared key s , Mallory cannot recover k_1 to generate a valid MAC (under standard security assumptions for the MAC function). This security property is similar to the one provided by the authenticated SLS in [28].

Detection of Fixed Power Attacks. Fixed power attacks are countered by the power randomization method that is employed in the second round of SecBeam. This is because

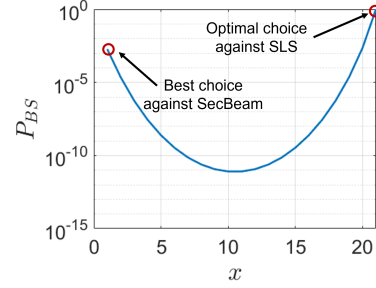


Fig. 11: P_{BS} when $N = 32$, $N_M = 21$ and $K = 19$.

when relaying SSFs at fixed power, the path loss test of Step 9 is violated. We demonstrate this in Proposition 1.

Proposition 1. *A fixed power attack on sector S_i is detected by the path loss test if the transmission power $P_i^T(2)$ in the second round satisfies*

$$P_i^T(2) < P_i^T(1) - \epsilon,$$

where ϵ is a noise-determined parameter.

Proof. The proof is provided in Appendix B. □

The intuition behind Proposition 1 is that by transmitting at a power lower than $P_i^T(1) - \epsilon$ in the second round, the path loss difference between the two rounds will violate the path loss test (will exceed ϵ) because the adversary relays at the same power, regardless of the transmission power of I . Parameter ϵ must be selected in such a way to account for the natural path loss variations between rounds. Such variations are expected to be primarily caused by noise, as the geometric properties of the mmWave channel lead to long coherence times in most environments of interest. We study the choice of ϵ in the evaluation via simulations and experiments.

Detection of Fixed Amplification Attacks. In a fixed amplification attack, Mallory applies a fixed gain to each sector she relays as opposed to transmitting at fixed power. Let Mallory receive from $N_M \leq N$ sectors during the first round initiator sector sweep, when $P_i^T = P_{\max}, \forall i$. Let also $K \leq N_M$ denote the sectors that, when amplified, achieve an SNR higher than the optimal sector without attack. The probability of passing the path loss test in the second round initiator sector sweep is given by Proposition 2.

Proposition 2. *Given the number of sectors N_M heard at \mathcal{M} and the number of sectors K in N_M with path loss smaller than the best path without attack under a fixed amplification strategy, the probability P_{BS} of a successful beam stealing attack is given by*

$$Pr_{BS} = \frac{1}{\binom{N_M}{x}^4} \cdot \left(\sum_{i=1}^{\min(x,K)} \binom{K}{i} \binom{N_M - K}{x - i} \right)^2.$$

Proof. The proof is provided in Appendix C. □

Discussion. The probability of success for the fixed amplification attack is a function of the number of sectors N_M

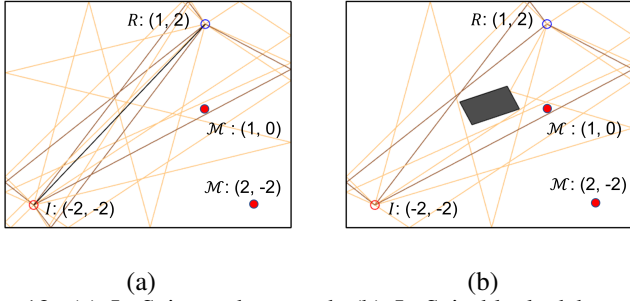


Fig. 12: (a) LoS is unobstructed, (b) LoS is blocked by an obstacle with permittivity equal to 2. \mathcal{M} was placed at two different locations.

heard at \mathcal{M} which is location- and wireless environment-dependent and the choice of x . It is evident that Pr_{BS} becomes 1 when $x = N_M$ (i.e., Mallory amplifies all sectors it hears in both rounds). The coarse AOA test is introduced to prevent the success of this strategy. When Mallory amplifies and relays all N_M sectors, the responder detects an unusual number of sectors arriving from the direction of the relay, thus detecting the attack. For values of x smaller than the coarse AoA test βN , the probability of success rapidly declines due to the requirement of relaying the same set of sectors on both rounds. In fact, based on the convexity of the binomial distribution [24], selecting $x = 1$ becomes Mallory's most beneficial strategy. In this case, the probability of success is $Pr_{BS} = K^2/N_M^4$.

As an example, Fig 11 shows P_{BS} , when $N = 32$, $N_M = 21$ and $K = 19$. With $\beta = 0.5$, Mallory must select $x < 16$ to pass the coarse AoA test with certainty. In this case, $x = 1$ yields the highest passing probability which is in the order of 10^{-3} . This is a fairly low probability for an online attack.

Another important remark for the analysis is that we have made the reasonable assumption of an adversary that does not know a priori the exact locations of I and R . Therefore she uses quasi-omni beams to the general directions of I and R in order to receive, amplify, and relay. If the adversary could exactly pinpoint I 's and R 's locations, she could point fine beams at each party, therefore substantially reducing the number of sectors N_M received by \mathcal{M} . In this case, relaying all N_M sectors passes the path lost test, while also defeating the coarse AoA test if $N_M < \beta N$.

VI. PARAMETER SELECTION AND EVALUATION

In this section, we use simulation based on ray-tracing (mmTrace) [29] to select parameters for SecBeam and evaluate its security. The insights from the simulations guide our experimental evaluations.

A. Simulation Setup

We consider two scenarios in our simulations, one where the LoS path between I and R is unobstructed (Fig. 12(a)), and the other one with the LoS blocked by an obstacle (Fig. 12(b)). All devices are placed in a self-defined room with a size of $5m \times 5m$, where the wall permittivity is set as 3.24. The

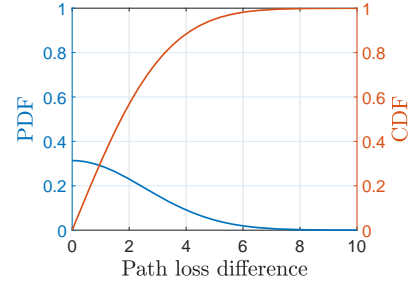


Fig. 13: PDF and CDF of ΔP given $\sigma = 1.8$

TABLE I: Simulation scenarios

	d_{IR}	d_{MR}	Room size	Amp.
Scenario 1	5m	1m	$5 \times 5 \times 5m$	40 dB
Scenario 2	5m	1m	$5 \times 5 \times 5m$	50 dB
Scenario 3	5m	1m	$5 \times 9 \times 5m$	40 dB
Scenario 4	5m	4.1m	$5 \times 5 \times 5m$	70 dB
Scenario 5	5m	5.4m	$9 \times 9 \times 9m$	70 dB

center coordinate of the room is set to $(0, 0)$, and the distance between I and R is $d_{IR} = 5m$. In addition, we consider two possible locations for \mathcal{M} : $(1, 0)$ and $(2, -2)$, which result in different distances between I , R , and \mathcal{M} , shown in Table II. Each device has N sectors in total, so the HPBW is $\lceil \frac{360^\circ}{N} \rceil$. Additionally, the HPBW of I and R 's quasi-omni pattern is 60° , and their maximum transmit power is $P_{max} = 0$ dBm. The initiator follows our protocol to perform the two-round sector sweep, using P_{max} in the first round and randomized power in the second round. The adversary implements the amplify-and-relay attack strategy with fixed amplification.

B. Parameter Selection

The SecBeam protocol is parameterized by the threshold of path loss difference ϵ and the frequency of one sector being chosen as the best receive sector β . In the following, we use simulations to help with selection of these parameters.

Selecting ϵ . The value of ϵ needs to be selected high enough to prevent false alarms when \mathcal{M} is not present. The path loss can be generally written as,

$$PL(dB) = G_T(dBi) + G_R(dBi) - L_{ch}(dB) + X_\sigma(dBm), \quad (1)$$

where P^T is the transmit power, G^T and G^R are the respective antenna gains, L_{ch} is the channel attenuation according to some unknown channel model, and X_σ is a zero-mean Gaussian noise with a standard deviation σ . Assuming fixed locations and paths, the path loss difference $\Delta P(dB)$ between the two rounds is,

$$\Delta P = |PL_i(2) - PL_i(1)| = |X_\sigma(2) - X_\sigma(1)|. \quad (2)$$

The path loss difference ΔP follows a folded normal distribution with a $\frac{\sigma\sqrt{2}}{\sqrt{\pi}}$ mean and $\sigma^2(1 - \frac{2}{\pi})$ variance. A typical value for σ in the indoor environment is 1.8 [38]. The probability density function (PDF) and the cumulative distribution function (CDF) of ΔP is shown in Fig. 13. In order to ensure a specific passing rate of valid devices, we can select a suitable value for ϵ based on the CDF of ΔP .

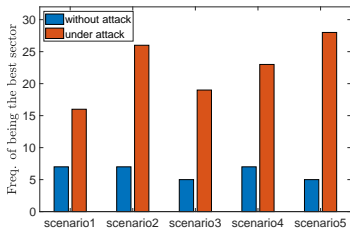


Fig. 14: The highest frequency of a sector being the best receive sector with and without \mathcal{M} in different scenarios.

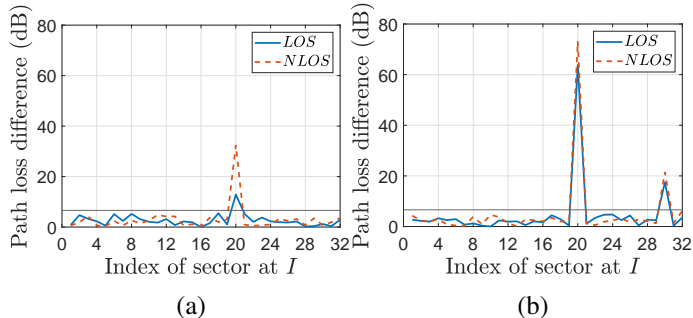


Fig. 15: Path loss difference with \mathcal{M} in LoS and NLoS scenarios: (a) \mathcal{M} chooses the same sector in two rounds of SSW, (b) \mathcal{M} chooses different sectors in two rounds of SSW.

For instance, in our study, we choose $\epsilon = 6.6\text{dB}$ to ensure that under benign conditions, the path loss difference due to noise is less than ϵ with probability 99%.

Selecting β . We then used our simulation results to determine the threshold τ . The optimal value of β depends on the physical environment. We listed five different simulation setups in Table. I where we vary the room size, locations of I and \mathcal{M} , and the amount of amplification (Amp.) used by \mathcal{M} . The total number of sectors is $N = 32$ in all scenarios. We extract the highest frequency $f_j, j = 1, \dots, N$ in each setup with and without a relay attack, and the results are shown in Fig. 14. In all the scenarios, there are a clear distinction between the beam selection frequencies of benign and adversarial settings, which shows the feasibility of the coarse AoA test.

In addition, we performed 1,000 simulations for $N = 16, 32$, and 64 with different combinations of the locations of I and R , room size, and amplification gain. The passing rate of legitimate devices and \mathcal{M} versus β is shown in Fig. 16. We can see that the passing rate of I and FA attacker (P_I and P_{FA}) both increase with β . When $\beta = 0.5$, $P_I = 1$ while $P_{FA} = 0$. So we conclude that $\beta = 0.5$ is sufficient to detect the attack for all values of N . It is worth mentioning that when the LoS between I and R is blocked, the frequency of one sector being selected as the best receive sector is higher than those shown in Fig. 14, since the LoS between \mathcal{M} and victims is always unobstructed. We discuss this in Sec. VI-C2.

C. Simulation Results

1) *Fixed power relay attack:* We use Setup 1 to demonstrate the security of SecBeam against the fixed power relay attack.

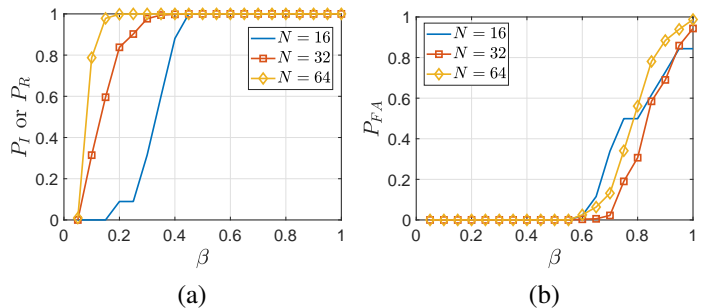


Fig. 16: Passing rates of a legitimate device (P_I or P_R) and \mathcal{M} (P_{FA}) versus β , for different N .

We show the results of the RSS measured by R in two rounds and the path loss difference when LoS is unobstructed and blocked in Fig. 17. From Fig. 17(a), sector 22 is chosen as the best sector in the first round, while in Fig. 17(c), the best sector is 30 because the LoS is blocked. We can also see that the path loss difference across two rounds is smaller than the threshold ϵ for all sectors, no matter whether the LoS is blocked or not.

When the adversary is present, the results are shown in Fig. 15. When \mathcal{M} chooses different sectors in two SSW rounds, e.g. sector 30 in the first round and sector 20 in the second round (Fig. 15(b)), the path loss difference exceeds ϵ in both cases. Even if \mathcal{M} could choose the same sector in two SSW rounds coincidentally, (e.g. Sector 20 in Fig. 15(a)), the path loss difference is still higher than ϵ due to the relay at fixed power and the power randomization by I .

2) *Fixed amplification attack:* Next, we show the simulation results when \mathcal{M} uses the fixed amplification relay strategy under simulation setup 2. We assume that \mathcal{M} amplifies all the received beams by 60 dB and relays them to R . When LoS is unobstructed, the results are shown in Fig. 18. From Fig. 18(a), we can see that in the benign case, even if some receive sectors, e.g. Sectors 6 and 8, are chosen more than once, $f_6 = 7/32$ and $f_8 = 7/32$ are less than the threshold $\beta = 0.5$. However, in Fig. 18(b) and (c), $f_{10} = 20/32$ under the FA attack, which is higher than the threshold, thus \mathcal{M} is detected. When the LoS is blocked, the results are shown in Fig. 19. In this case, there is no dominant path between I and R , and the obstacle acts as a reflector. The best receive sector does not present any strong directionality. Comparing with Fig. 18(b) and (c), we can observe sector 10 is the best receive sector for 29 transmit sectors in Fig. 19(b) and 19(c) as expected.

VII. EXPERIMENTAL EVALUATION

A. Experimental Setup

To demonstrate the effectiveness and security of SecBeam in the real world, we implemented it using our mmWave testbed as described in Section III-A.

Figure 20 provides an overview of the experimental setup, where d_{IM} was 3m and d_{MR} was 2.4m. To increase the number of reflection paths in the environment, in certain

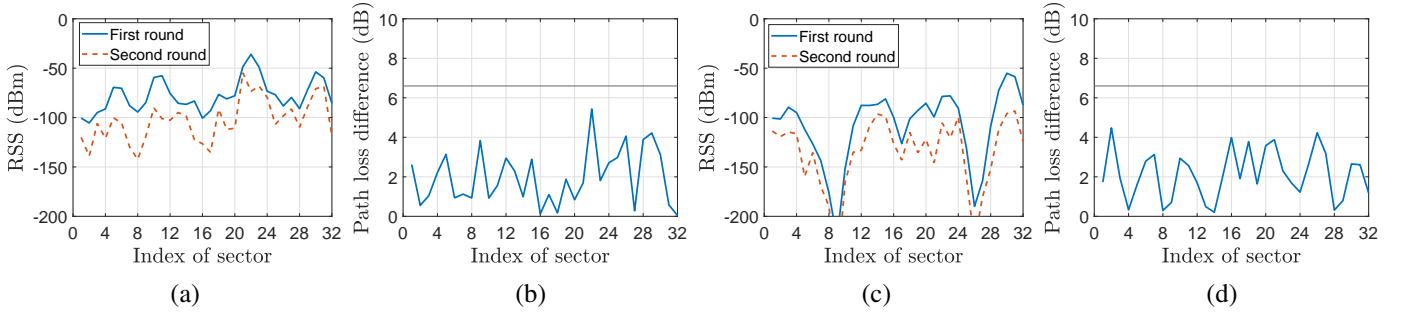


Fig. 17: Simulation results without \mathcal{M} : (a) RSS measured by R when LoS is unobstructed, (b) path loss difference between two rounds when LoS is unobstructed, (c) RSS measured by R when LoS is blocked, (d) path loss difference between two rounds when LoS is blocked. The path loss difference is lower than the threshold in both LoS and NLoS scenarios.

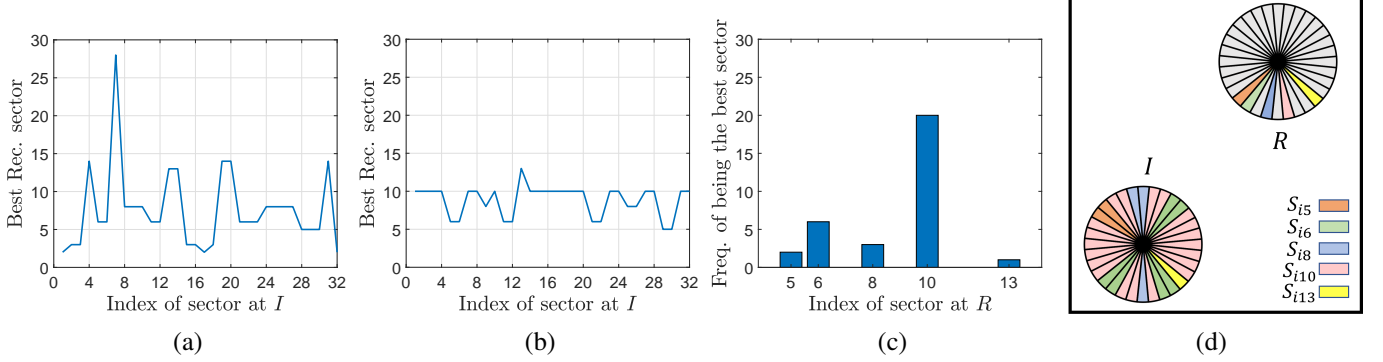


Fig. 18: When LoS between I and R is unobstructed:(a) The best Tx and Rx pair S_{ij} without relay attack. (b) S_{ij} under relay attack. (c) the frequency of a Rx sector being chosen as the best receive sector under relay attack. (d) S_{ij} in a real setting.

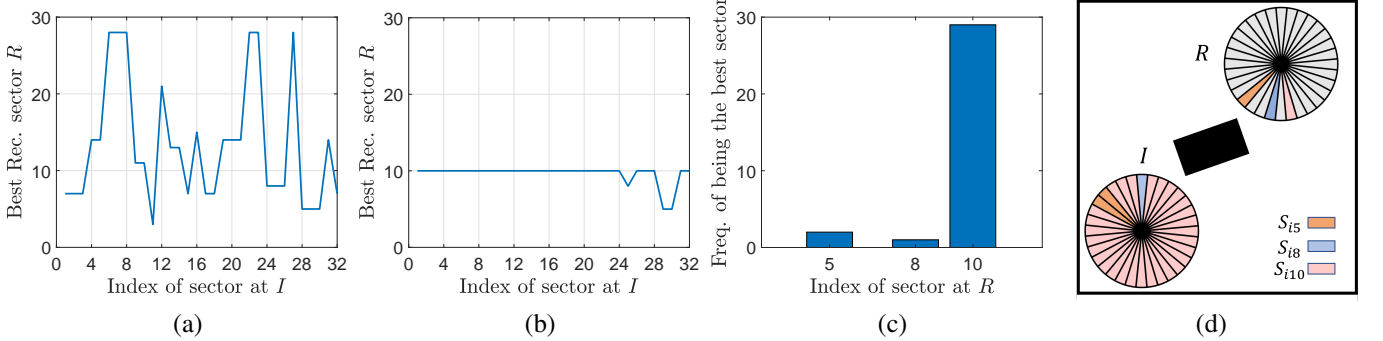


Fig. 19: When LoS between I and R is blocked:(a) The best Tx and Rx pair S_{ij} without relay attack. (b) S_{ij} under relay attack. (c) the frequency of an Rx sector being chosen as the best receive sector under relay attack. (d) S_{ij} in a real setting. Sectors at RX are the best receive sectors for the transmit sectors indicating in the same color in Tx.

setups, we added a whiteboard and a stop sign in the room. The relay attack was implemented by synchronizing \mathcal{M} , I and R via the Octo-clock module. This way the adversary could transmit the same SSF frame synchronously with the legitimate devices, without incurring the hardware delay of USRPs for switching between reception and transmission.

During the experiments, the transmitter sent 10,000 packets in each sector with a 5 milliseconds delay between packets to facilitate data collection (In reality, only one packet will be sent in each sector). In the first round, I swept in its maximum transmit power $P_{max} = 30\text{dBm}$. In the second round, I randomly chose the transmit power sequence for each sector. For the fixed power relay attack, the adversary

chose signals from one Tx sector and relayed them to the receiver using P_{max} . For the fixed amplification relay attack, \mathcal{M} amplified its received signals from I with a fixed amount and then relayed them to R .

B. Security Evaluation of SecBeam

1) Security against the fixed power relay attack: In our experimental setup, there are 7 transmit sectors that can be detected by R in the first round of sector sweep. The transmit powers for each sector are randomly chosen as $P_i^T(2) = \{16, 7, 22, 0, 10, 9, 18, 19, 4, 11, 10, 15\}\text{dBm}$ in the second round of sector sweep. The SNR measured at R in two rounds of SSW consist of two matrices of dimension



Fig. 20: Experimental setup.

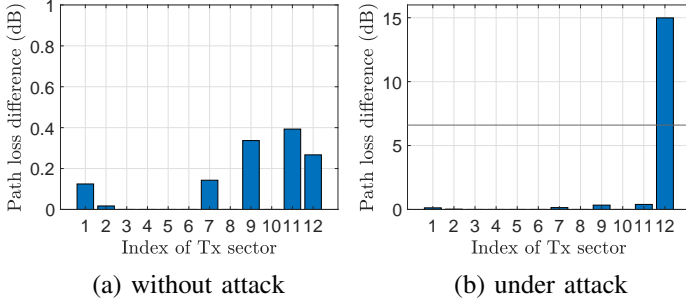


Fig. 21: Path loss difference without and under attack during the initiator sector sweep phase.

10,000 \times 7. Using these SNR data and the known transmit power values, we calculated the average path loss differences over 10000 measurements for each sector, shown in Fig. 21. We observe that when there is no adversary present, the average path loss difference for all sectors remains under 0.5 dB, and all 10000 path loss differences for each transmit sector are smaller than the threshold $\epsilon = 6.6$. However, when the *FP* attack is carried out, the average path loss difference for the affected sector (r_{12} in this example) is 14.9875 dB, which is greater than $\epsilon = 6.6$.

2) *Security against fixed amplification relay attack*: We first present the frequency of any receive sector being chosen as the best sector for legitimate devices, as illustrated in Figure 22. From Fig. 22(a), when the artificial reflectors are present in the environment, the frequency of choosing sector 7 at R as the best sector is found to be $f_7 = 3/12$. However, after removing the reflectors, in Figure 22(b), sector 7 at R was chosen 4 times out of 12 as the best receiving sector, resulting in $f_7 = 4/12$. The values of f_7 in both environments are lower than the threshold β , which indicates that the legitimate devices can pass the coarse AoA test.

In the presence of an adversary, we conduct an experiment where the adversary attempts to relay all the received signals to the intended receiver R . Our experimental results, as shown in Fig. 23, revealed that the probability of the adversary successfully relaying signals to R from sector 3 was high ($f_3 = 9/12$) and exceeded the threshold value of $\beta = 0.5$, indicating that the *FA* attack is detected. We show the best transmit and receive beam pair S_{ij} for this setup in Fig. 23(c). The black sectors in Fig. 23(c) means that signals sent using

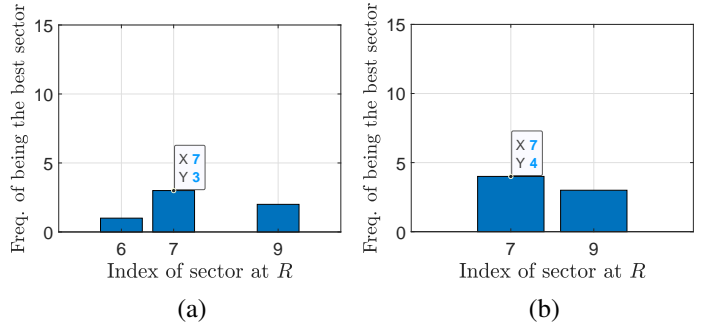


Fig. 22: Experimental results without \mathcal{M} : (a) frequency of a sector being chosen as the best receive sector with artificial reflectors, (b) Frequency of a sector being chosen as the best receive sector without the artificial reflectors.

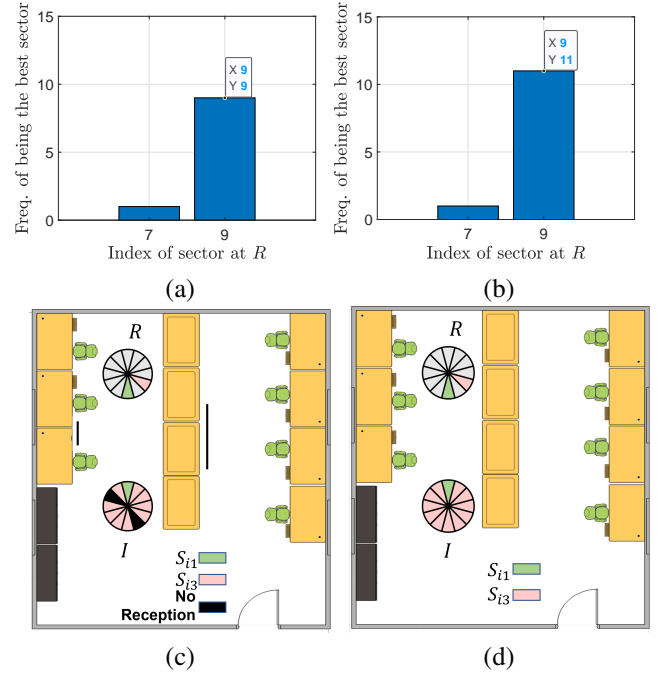


Fig. 23: Experimental results under *FA* relay attack: (a) Frequency of a sector being chosen as the best receive sector when artificial reflectors are in the environment. (b) Frequency of a sector being chosen as the best receive sector without artificial reflectors. (c) S_{ij} on real mmWave devices with artificial reflectors. (d) S_{ij} on real mmWave devices without artificial reflectors.

these sectors cannot be received by R . When we removed the reflectors, f_3 further increased to 11/12 as shown in Figs. 23(b) and (d), which is above the threshold value of β . The adversary is detected.

C. Time Efficiency of SecBeam

The run time of SecBeam is dominated by the number of sectors at the devices. The time required for RSS and AoA measurements is negligible. Let the size of each sector sweep frame be F bytes, the number of frames sent by each sector be Y , bandwidth be BW , both I and R have N_q quasi-omni patterns, the time interval between frames sent by the same

antenna, Short Beamforming Interframe Spacing (SBIFS), be T_S and the time consumed to switch quasi-omni pattern, Long Beamforming Interframe Spacing (LBIFS), be T_L . The total time for protocol execution is computed as $2N_q(N(\frac{YF}{BW} + (Y-1)T_S) + (N-N_q)T_S + (N_q-1)T_L) + 2(N_q-1)T_L$. If we assume $F = 26$, $Y = 1$, $T_S = 1\mu s$, and $T_L = 18\mu s$ as defined in the 802.11ad standard [14], $N = 32$, $N_q = 6$, and $BW = 160$ MHz, the total time consumed by SecBeam is 2.07 ms.

VIII. RELATED WORK

Relay attacks. The amplify-and-forward beam stealing attacks is a relay type of attack. However, existing relay attacks against wireless systems have different purpose. The majority of relay attacks aim at violating the proximity/distance constraint between two devices (a prover and a verifier), for applications where proximity-based access control is needed. For example, keyless entry and start systems for cars [8], [9], contactless payment systems with smartcards/RFID [17], etc. We emphasize that the beam-stealing attack differs from the above relay attacks, since it aims at distorting the path-loss property rather than proximity or distance. In addition, there is no location restriction imposed on the attacker.

There is also another type of relay attack in the literature, namely signal cancellation/annihilation attack [5], [12], [21], [23], where the attacker aims at causing destructive interference at the intended receiver(s) of a wireless communication link, which either leads to denial-of-service, or can be used to achieve message modification via arbitrary bit flips. However, signal cancellation is generally hard to carry out since it requires precise timing and phase synchronization, which is also more challenging in mmWave communication systems due to the directionality of the beams. In contrast, the amplify-and-forward beam stealing attack is a form of MitM attack which disrupts beam selection so that the attacker has full control of the communication link between the legitimate devices (it can eavesdrop, modify, or perform DoS against the messages exchanged). In addition, it is easier to implement than signal cancellation.

Relay Attack Defenses. Existing defenses against relay attacks are not applicable to defend against beam-stealing attacks in general. For example, distance bounding protocols [3], [6], [7] aim at enforcing a lower-bound of the distance from a prover to the verifier. However, we target general communication scenarios where no proximity/distance bound is imposed on the communicating devices. Although one can also use distance bounding as a secure signal path length measurement to indirectly prove that no longer paths than the dominating path (e.g., LoS) has a lower path-loss, implementing distance bounding typically requires advanced hardware capabilities [32]. Moreover, I and R have no knowledge of the wireless environment. If a stronger signal appears on a longer path, this could be because the shorter path experiences higher absorption or diffraction if it is not the LoS.

Existing relay attacks can also be detected by verifying the co-presence of devices via some common context, such as

ambient conditions (e.g., sound, lighting, motion, RF signals, etc) [19], [20], [33], [34], [40]. However, as stated earlier, they are not applicable to defend beam-stealing attacks due to the different purpose and assumptions of the attack.

On the other hand, another category of defenses utilize physical-layer identification/RF fingerprinting methods to identify the transmitting devices (or fingerprint the channel between the devices) via their signal characteristics, in order to detect impersonation attacks or distinguish different devices. For example, Balakrishnan *et al.* [4] fingerprint mmWave devices based on features extracted from their spatial-temporal beam patterns and demonstrated the resistance of their protocol against impersonation attacks. Wang *et al.* [35], [36] adopted a similar idea, and utilized machine learning algorithms to identify each device based on its unique beam pattern. Although these methods can be applicable to detect beam-stealing attacks, they all require a prior (secure) training phase to extract beam patterns of known devices, which not only brings extra overhead but also does not work well when the channel condition changes or new devices are introduced to the network. In contrast, our proposed defense, SecBeam does not require any prior knowledge about the devices or channel environment.

Finally, we are aware of only one work that proposed a specific defense against the beam-stealing attack under the IEEE 802.11ad protocol (Steinmetzer *et al.* [28]). Since the original SLS protocol in IEEE 802.11ad is unauthenticated which allows beam-stealing by simply modifying the SSW messages, they integrated crypto machinery into the sector sweep process, in order to authenticate the SSW messages, which prevents the simple form of beam-stealing attacks. However, as we demonstrated in this paper, it is still vulnerable to amplify-and-relay beam-stealing attacks. It is an open problem to defend against such attacks.

IX. CONCLUSIONS AND FUTURE WORK

In this paper, we studied the security of the 802.11ad beam alignment protocol for mmWave communications. Although prior work have added cryptographic protection to secure beam alignment messages, we demonstrate that this protocol is still vulnerable to a new amplify-and-relay beam stealing attack that does not require message forging and bypasses cryptographic protections. We then propose a new secure beam sweeping protocol, SecBeam, which exploits power/sector randomization and coarse angle-of-arrival information to detect amplify-and-relay attacks. Essentially, SecBeam constructs a physical layer commitment scheme that commits to the path loss of each beam. SecBeam does not require any prior knowledge of the physical environment and is compatible with the current 802.11ad standard. We theoretically analyzed the security of SecBeam, and used both ray-tracing simulations and real-world experiments on a mmWave testbed to evaluate the security of our protocol. Results show that SecBeam can detect two different types of amplify-and-relay attacks under realistic scenarios. Future works will include extending our

method to other efficient beam alignment protocols beyond 802.11ad, for example, protocols with sub-linear complexity.

REFERENCES

- [1] [Online]. Available: <https://www.ettus.com/all-products/usrp-n320/>
- [2] [Online]. Available: <https://tmytek.com/products/frequency-converters/udbox5g>
- [3] A. Abidin, “Quantum distance bounding,” in *Proceedings of the 12th Conference on Security and Privacy in Wireless and Mobile Networks*, 2019, pp. 233–238.
- [4] S. Balakrishnan, S. Gupta, A. Bhuyan, P. Wang, D. Koutsonikolas, and Z. Sun, “Physical layer identification based on spatial-temporal beam features for millimeter-wave wireless networks,” *IEEE Transactions on Information Forensics and Security*, vol. 15, pp. 1831–1845, 2019.
- [5] S. Čapkun, M. Čagalj, R. Rengaswamy, I. Tsigkogiannis, J.-P. Hubaux, and M. Srivastava, “Integrity codes: Message integrity protection and authentication over insecure channels,” *IEEE Transactions on Dependable and Secure Computing*, vol. 5, no. 4, pp. 208–223, 2008.
- [6] C. Cremers, K. B. Rasmussen, B. Schmidt, and S. Capkun, “Distance hijacking attacks on distance bounding protocols,” in *2012 IEEE Symposium on Security and Privacy*. IEEE, 2012, pp. 113–127.
- [7] S. Drimer, S. J. Murdoch *et al.*, “Keep your enemies close: Distance bounding against smartcard relay attacks,” in *USENIX security symposium*, vol. 312, 2007.
- [8] A. Francillon, B. Danev, and S. Capkun, “Relay attacks on passive keyless entry and start systems in modern cars,” in *Proceedings of the Network and Distributed System Security Symposium (NDSS)*. Eidgenössische Technische Hochschule Zürich, Department of Computer Science, 2011.
- [9] L. Francis, G. Hancke, K. Mayes, and K. Markantonakis, “Practical relay attack on contactless transactions by using nfc mobile phones,” *Cryptology ePrint Archive*, 2011.
- [10] H. Gao, W. Wang, Y. Wu, Y. Liu, G. F. Pedersen, and W. Fan, “Experimental comparison of on-off and all-on calibration modes for beam-steering performance of mmwave phased array antenna-in-package,” *IEEE Transactions on Instrumentation and Measurement*, vol. 70, pp. 1–9, 2021.
- [11] Y. Ghasempour, C. R. Da Silva, C. Cordeiro, and E. W. Knightly, “Ieee 802.11 ay: Next-generation 60 ghz communication for 100 gb/s wi-fi,” *IEEE Communications Magazine*, vol. 55, no. 12, pp. 186–192, 2017.
- [12] N. Ghose, L. Lazos, and M. Li, “Help: Helper-enabled in-band device pairing resistant against signal cancellation,” in *USENIX Security Symposium*, 2017, pp. 433–450.
- [13] P. Gupta and S. Kar, “Music and improved music algorithm to estimate direction of arrival,” in *2015 International Conference on Communications and Signal Processing (ICCCSP)*. IEEE, 2015, pp. 0757–0761.
- [14] *IEEE Standard for Information technology–Telecommunications and information exchange between systems–Local and metropolitan area networks–Specific requirements–Part 11: Wireless LAN Medium Access Control (MAC) and Physical Layer (PHY) Specifications Amendment 3: Enhancements for Very High Throughput in the 60 GHz Band*, IEEE Std. IEEE 802.11ad, 2012.
- [15] F. Jameel, S. Wyne, S. J. Nawaz, and Z. Chang, “Propagation channels for mmwave vehicular communications: State-of-the-art and future research directions,” *IEEE Wireless Communications*, vol. 26, no. 1, pp. 144–150, 2018.
- [16] Z. Jiang, T. H. Luan, X. Ren, D. Lv, H. Hao, J. Wang, K. Zhao, W. Xi, Y. Xu, and R. Li, “Eliminating the barriers: demystifying wi-fi baseband design and introducing the picoscenes wi-fi sensing platform,” *IEEE Internet of Things Journal*, vol. 9, no. 6, pp. 4476–4496, 2021.
- [17] Z. Kfir and A. Wool, “Picking virtual pockets using relay attacks on contactless smartcard,” in *First International Conference on Security and Privacy for Emerging Areas in Communications Networks (SECURECOMM’05)*. IEEE, 2005, pp. 47–58.
- [18] M. Kim, E. Hwang, and J.-N. Kim, “Analysis of eavesdropping attack in mmwave-based wpans with directional antennas,” *Wireless Networks*, vol. 23, no. 2, pp. 355–369, 2017.
- [19] D. Ma, A. K. Prasad, N. Saxena, and T. Xiang, “Location-aware and safer cards: enhancing rfid security and privacy via location sensing,” in *Proceedings of the fifth ACM conference on Security and Privacy in Wireless and Mobile Networks*, 2012, pp. 51–62.
- [20] S. Mathur, R. Miller, A. Varshavsky, W. Trappe, and N. Mandayam, “Proximate: proximity-based secure pairing using ambient wireless signals,” in *Proceedings of the 9th international conference on Mobile systems, applications, and services*, 2011, pp. 211–224.
- [21] D. Moser, V. Lenders, and S. Capkun, “Digital radio signal cancellation attacks: An experimental evaluation,” in *Proceedings of the 12th conference on security and privacy in wireless and mobile networks*, 2019, pp. 23–33.
- [22] E. Papadogiannaki and S. Ioannidis, “A survey on encrypted network traffic analysis applications, techniques, and countermeasures,” *ACM Computing Surveys (CSUR)*, vol. 54, no. 6, pp. 1–35, 2021.
- [23] C. Pöpper, N. O. Tippenhauer, B. Danev, and S. Capkun, “Investigation of signal and message manipulations on the wireless channel,” in *Computer Security–ESORICS 2011: 16th European Symposium on Research in Computer Security, Leuven, Belgium, September 12–14, 2011. Proceedings 16*. Springer, 2011, pp. 40–59.
- [24] L. T. RAMSEY, “Convexity of the binomial distribution,” 2005.
- [25] T. S. Rappaport, *Wireless communications: Principles and practice*, 2/E. Pearson Education India, 2010.
- [26] T. S. Rappaport, Y. Xing, G. R. MacCartney, A. F. Molisch, E. Mellios, and J. Zhang, “Overview of millimeter wave communications for fifth-generation (5g) wireless networks—with a focus on propagation models,” *IEEE Transactions on Antennas and Propagation*, vol. 65, no. 12, pp. 6213–6230, 2017.
- [27] M. K. Samimi, G. R. MacCartney, S. Sun, and T. S. Rappaport, “28 ghz millimeter-wave ultrawideband small-scale fading models in wireless channels,” in *2016 IEEE 83rd Vehicular Technology Conference (VTC Spring)*. IEEE, 2016, pp. 1–6.
- [28] D. Steinmetzer, S. Ahmad, N. Anagnostopoulos, M. Hollick, and S. Katzenbeisser, “Authenticating the sector sweep to protect against beam-stealing attacks in ieee 802.11 ad networks,” in *Proceedings of the 2nd ACM Workshop on Millimeter Wave Networks and Sensing Systems*, 2018, pp. 3–8.
- [29] D. Steinmetzer, J. Classen, and M. Hollick, “mmtrace: Modeling millimeter-wave indoor propagation with image-based ray-tracing,” in *2016 IEEE conference on computer communications workshops (INFOCOM WKSHPs)*. IEEE, 2016, pp. 429–434.
- [30] D. Steinmetzer, Y. Yuan, and M. Hollick, “Beam-stealing: Intercepting the sector sweep to launch man-in-the-middle attacks on wireless ieee 802.11 ad networks,” in *Proceedings of the 11th ACM Conference on Security & Privacy in Wireless and Mobile Networks*, 2018, pp. 12–22.
- [31] X. Tian, Q. Liu, Z. Wang, and M. Li, “Secure hybrid beamformers design in mmwave mimo wiretap systems,” *IEEE Systems Journal*, vol. 14, no. 1, pp. 548–559, 2019.
- [32] N. O. Tippenhauer, H. Luecken, M. Kuhn, and S. Capkun, “Uwb rapid-bit-exchange system for distance bounding,” in *Proceedings of the 8th ACM Conference on Security & Privacy in Wireless and Mobile Networks*, 2015, pp. 1–12.
- [33] H. T. T. Truong, X. Gao, B. Shrestha, N. Saxena, N. Asokan, and P. Nurni, “Comparing and fusing different sensor modalities for relay attack resistance in zero-interaction authentication,” in *2014 IEEE International Conference on Pervasive Computing and Communications (PerCom)*. IEEE, 2014, pp. 163–171.
- [34] P. Urien and S. Piramuthu, “Elliptic curve-based rfid/nfc authentication with temperature sensor input for relay attacks,” *Decision Support Systems*, vol. 59, pp. 28–36, 2014.
- [35] N. Wang, L. Jiao, P. Wang, W. Li, and K. Zeng, “Machine learning-based spoofing attack detection in mmwave 60ghz ieee 802.11 ad networks,” in *IEEE INFOCOM 2020-IEEE Conference on Computer Communications*. IEEE, 2020, pp. 2579–2588.
- [36] —, “Exploiting beam features for spoofing attack detection in mmwave 60-ghz ieee 802.11 ad networks,” *IEEE Transactions on Wireless Communications*, vol. 20, no. 5, pp. 3321–3335, 2021.
- [37] Y. Wang, Z. Wei, and Z. Feng, “Beam training and tracking in mmwave communication: A survey,” 2022.
- [38] X. Wu, Y. Zhang, C.-X. Wang, G. Goussetis, M. M. Alwakeel *et al.*, “28 ghz indoor channel measurements and modelling in laboratory environment using directional antennas,” in *2015 9th European Conference on Antennas and Propagation (EuCAP)*. IEEE, 2015, pp. 1–5.
- [39] M. Xiao, S. Mumtaz, Y. Huang, L. Dai, Y. Li, M. Matthaiou, G. K. Karagiannidis, E. Björnson, K. Yang, C.-L. I, and A. Ghosh, “Millimeter wave communications for future mobile networks,” *IEEE Journal on Selected Areas in Communications*, vol. 35, no. 9, pp. 1909–1935, 2017.

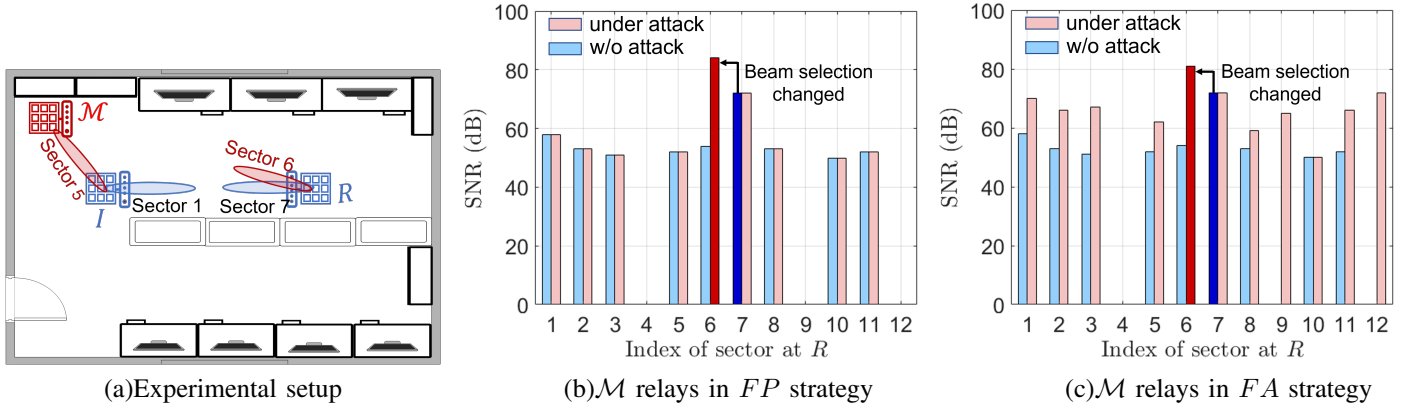


Fig. 24: Amplify-and-relay beam-stealing attack setup and experimental results when \mathcal{M} uses FA and FP relay strategies. R chooses sector 7 without \mathcal{M} , and sector 6 when \mathcal{M} relays in either FA or FP strategies.

- [40] Z. Xu, J. Li, Y. Pan, L. Lazos, M. Li, and N. Ghose, "PoF: Proof-of-following for vehicle platoons," in *Proceedings 2022 Network and Distributed System Security Symposium*, 2022.
- [41] Y. Yang, X. Wei, R. Xu, L. Peng, L. Zhang, and L. Ge, "Man-in-the-middle attack detection and localization based on cross-layer location consistency," *IEEE Access*, vol. 8, pp. 103 860–103 874, 2020.
- [42] Y. Zhu, L. Wang, K.-K. Wong, and R. W. Heath, "Secure communications in millimeter wave ad hoc networks," *IEEE Transactions on Wireless Communications*, vol. 16, no. 5, pp. 3205–3217, 2017.

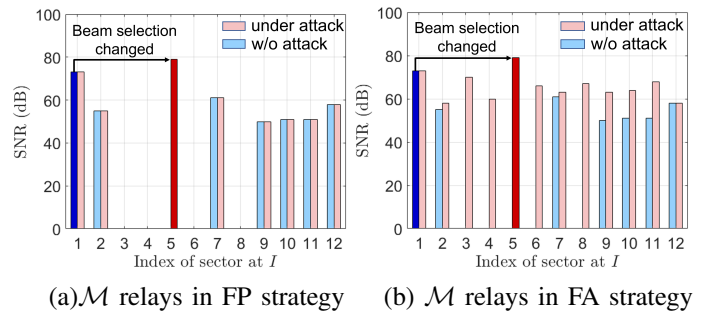


Fig. 25: Amplify-and-relay beam stealing attack on I using FA and FP strategies. I chooses sector 1 without \mathcal{M} , and sector 5 when \mathcal{M} relays in either FA or FP strategies.

APPENDIX

A. Amplify-and-Relay Beam-Stealing Attack in Setup 2

The experimental setup, illustrated in Fig. 24(a), consists of devices that are located at distances of $d_{IM} = 2.7m$, $d_{IR} = 4.3m$, and $d_{MR} = 6m$. To achieve synchronization between devices I and \mathcal{M} , an external clock (Ettus OctoClock-G) is used. In this configuration, \mathcal{M} and R are situated in different quasi-omni patterns of I , enabling \mathcal{M} to relay sector sweep frames from R to I while I is receiving in the quasi-omni pattern towards itself. Consequently, there is no need to synchronize \mathcal{M} and R . The results of this setup are shown in Fig. 24(b)(c) and Fig. 25. When there is no adversary, I and R select sector 1 and sector 7 as the best beam pair.

Fig. 24(b) and Fig. 25(a) demonstrate the impact of \mathcal{M} relaying using FP strategy, leading to R and I switching to sector 6 and sector 5, respectively. In Fig. 24(c) and Fig. 25(b), \mathcal{M} relays using FA strategy, resulting in the selection of sector 5 at I and sector 6 at R again. Ultimately, \mathcal{M} successfully directs I and R to choose beams pointing towards him in both strategies. We further verified that without \mathcal{M} , I and R were unable to communicate using sector 5 and sector 6. These results are in line with those presented in Sec. III-A.

B. Proof of Proposition 1

Proposition 1. A fixed power attack on sector S_i is detected by the path loss test if the transmission power $P_i^T(2)$ in the second round satisfies

$$P_i^T(2) < P_i^T(1) - \epsilon,$$

where ϵ is a noise-determined parameter.

Proof. Consider the transmission of an SSF at sector S_i by I during the first round with power $P_i^T(1)$. The path loss calculated by R is $PL_i(1)(dB) = P_i^T(1)(dBm) - P_i^R(1)(dBm)$. Similarly, R calculates the path loss of the second round as $PL_i(2)(dB) = P_i^T(2)(dBm) - P_i^R(2)(dBm)$. Taking the absolute difference yields

$$\begin{aligned} |PL_i(1) - PL_i(2)| &= PL_i(1) - PL_1(2) \\ &= P_i^T(1) - P_i^R(1) - P_i^T(2) + P_i^R(2) \\ &> P_i^T(1) - P_i^T(1) + \epsilon \\ &> \epsilon. \end{aligned} \quad (3)$$

In (3), we used the fact that $PL_i(1) > PL_1(2)$ because I 's transmission power is reduced in the second round whereas Mallory transmits at fixed power thus leading to the calculation of lower path loss. Moreover, because Mallory's transmission is at fixed power, it follows that $P_i^R(1) = P_i^R(2)$. Finally, by design, $P_i^T(2) < P_i^T(1) - \epsilon$. \square

C. Proof of Proposition 2

Proposition 2. Given the number of sectors N_M heard at \mathcal{M} and the number of sectors K in N_M with path loss smaller than the best path without attack under a fixed amplification strategy, the probability P_{BS} of a successful beam stealing attack is given by

$$Pr_{BS} = \frac{1}{\binom{N_M}{x}^4} \cdot \left(\sum_{i=1}^{\min(x,K)} \binom{K}{i} \binom{N_M - K}{x - i} \right)^2.$$

Proof. To prove Proposition 2, we first describe the adversary's strategy. During the first round, Mallory must choose which SSFs out of the N_M ones that she receives should be amplified and forwarded to R . Given the online nature of the attack, this decision is made in real time. Let Mallory decide to forward x out of the N_M sectors, without being able to identify them since the sector IDs are encrypted. The probability of choosing at least one sector that can defeat the optimal legitimate sector without attack (and therefore steal the beam) is given by the probability that any of the K amplified sectors that defeat the optimal one are chosen. We compute this probability as

$$Pr_1 = \sum_{i=1}^{\min\{x,K\}} \frac{\binom{K}{i} \cdot \binom{N_M - K}{x - i}}{\binom{N_M}{x}}. \quad (4)$$

Equation (4) is the enumeration of all possible ways of choosing exactly i sectors out of K , when Mallory chooses to amplify x out of N_M sectors at random. In the second round, \mathcal{M} has to amplify exactly the same x sectors to pass the path

loss test. If any sector out of the x amplified in round 1 is not amplified in the second round, the path loss calculated for that sector will differ by the amplification gain applied in the first round.

However, the sweep sequence is randomized in the second round by the application of the pseudorandom permutation Π . Moreover, Mallory cannot decrypt SSFs to recover the sector ID. Even if she could, the online nature of the attack does not permit enough time for frame decoding. Therefore, the probability of passing the path loss test is given by the probability of selecting the same set of x SSFs, given by $Pr_2 = 1/\binom{N_M}{x}$. Combining the events of choosing a sector that defeats the optimal one in the first round and choosing the same sectors to amplify in the second round yields Mallory's success probability in stealing the initiator's beam

$$Pr_{FA} = \frac{1}{\binom{N_M}{x}^2} \cdot \left(\sum_{i=1}^{\min(x,K)} \binom{K}{i} \binom{N_M - K}{x - i} \right) \quad (5)$$

To successfully steal the beams in both directions, \mathcal{M} must succeed in both the initiator and responder sector sweep processes. This probability is given by $Pr_{BS} = (Pr_{FA})^2$. \square